

# Flexible Light-Emitting Diodes Based on Vertical Nitride Nanowires

Xing Dai,<sup>\*,†</sup> Agnes Messanvi,<sup>‡,§,§</sup> Hezhi Zhang,<sup>†</sup> Christophe Durand,<sup>‡,§</sup> Joël Eymery,<sup>‡,§</sup> Catherine Bougerol,<sup>‡,||</sup> François H. Julien,<sup>†</sup> and Maria Tchernycheva<sup>\*,†</sup>

<sup>†</sup>Institut d'Electronique Fondamentale, UMR 8622 CNRS, University Paris Sud XI, 91405 Orsay, France

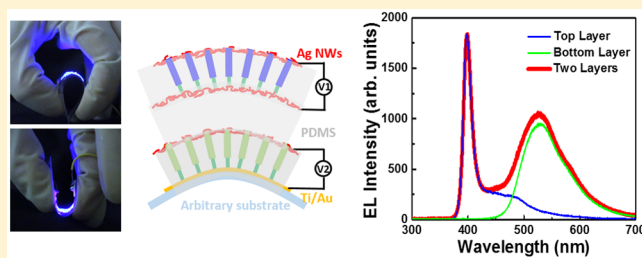
<sup>‡</sup>Université Grenoble Alpes, 38000 Grenoble, France

<sup>§</sup>“Nanophysique et Semiconducteurs” group, CEA, INAC-SP2M, 17 Avenue des Martyrs, 38000 Grenoble, France

<sup>||</sup>“Nanophysique et Semiconducteurs” group, CNRS, Institut Néel, 25 Avenue des Martyrs, 38000 Grenoble, France

## Supporting Information

**ABSTRACT:** We demonstrate large area fully flexible blue LEDs based on core/shell InGaN/GaN nanowires grown by MOCVD. The fabrication relies on polymer encapsulation, nanowire lift-off and contacting using silver nanowire transparent electrodes. The LEDs exhibit rectifying behavior with a light-up voltage around 3 V. The devices show no electroluminescence degradation neither under multiple bending down to 3 mm curvature radius nor in time for more than one month storage in ambient conditions without any protecting encapsulation. Fully transparent flexible LEDs with high optical transmittance are also fabricated. Finally, a two-color flexible LED emitting in the green and blue spectral ranges is demonstrated combining two layers of InGaN/GaN nanowires with different In contents.



EL Intensity (arb. units)

Wavelength (nm)

Blue Layer

Green Layer

Two Layers

**KEYWORDS:** Nanowires, nitrides, light emitting diodes, color-tunable emitters, flexible devices, organic/inorganic hybrid devices

Flexible light-emitting diodes (LEDs) are today a topic of intense research, motivated by their numerous economically relevant applications (e.g., rollable displays, wearable intelligent electronics, lightning, and so forth). Presently, flexible devices mainly use organic materials integrated on lightweight and flexible plastic substrates. Thanks to the flexibility, relative ease of processing, compatibility with various flexible substrates, and their low cost, organic LEDs (OLEDs) are today the key technology for flexible displays. In the past decades, the OLED performance has been tremendously improved.<sup>1–4</sup> However, they still face the issue of a poor time stability caused by the degradation of the electrical conductivity of the organic layers and of the interface degradation in the active region.<sup>5–7</sup> Especially, OLEDs present limitations in the short wavelength range, which has a detrimental influence on the color balance of the displays. Indeed, blue OLEDs suffer from a rather low luminance (around  $10^2$ – $10^4$  cd/m<sup>2</sup>),<sup>3,8</sup> low external quantum efficiency (EQE) (e.g., 2–30%),<sup>9</sup> and a limited lifetime (e.g., up to 3700 h for T50, time to 50% of initial luminance of 1000 cd/m<sup>2</sup>).<sup>4</sup>

Today, the technology providing the best performance in terms of luminance and EQE in the blue spectral range relies on nitride semiconductors. Indeed, InGaN/GaN LEDs demonstrate a high luminance of several  $10^6$  cd/m<sup>2</sup>,<sup>10,11</sup> an EQE above 80%,<sup>12</sup> and a lifetime of more than 100,000 h. Several attempts have been performed to fabricate flexible LEDs based on nitride thin films.<sup>13–16</sup> However, the fabrication of flexible devices from conventional thin film structures is quite challenging and requires additional processing steps to

microstructure the active layer. Nitride micropyramid arrays with a rather large pyramid size above 10  $\mu\text{m}$  have also been used to demonstrate a flexible LED by developing a special method to transfer micropyramids onto plastic.<sup>17</sup> To further improve the flexibility, it is advantageous to shrink the active element dimensions and to use bottom-up nanostructures such as nanowires.

Nitride nanowires show remarkable mechanical and optoelectronic properties stemming from their high aspect-ratio. They are mechanically flexible and can stand high deformations without plastic relaxation.<sup>18</sup> The nanowires also allow the significant improvement of the material quality by reducing the dislocation density and relaxing the strain induced by thermal expansion mismatch.<sup>19</sup> For light-emitting devices, the nanowires can facilitate the light extraction because of their wave guiding properties.<sup>20</sup> Moreover, core/shell nanowire structures provide further advantage of increasing the active device area and of suppressing the quantum confined Stark effect.<sup>21,22</sup> Single nanowire LEDs dispersed on both rigid<sup>23–25</sup> and flexible plastic substrates<sup>26</sup> have been investigated, but the complexities in positioning single nanowires and integrating with nonconventional substrates restrict their widespread applications. Meanwhile, nanowire array LEDs based on InGaN/GaN heterostructures have also been successfully demonstrated on

**Received:** July 23, 2015

**Revised:** August 27, 2015

**Published:** August 31, 2015

rigid substrates, showing excellent performances in the blue spectral range.<sup>21,27–31</sup>

Thanks to this promising performance of nanowire LEDs, polymer-embedded nanowires offer an elegant solution to create a light emitter, which combines the high brightness and the long lifetime of inorganic semiconductor materials with the high flexibility of polymers. Nanowire arrays embedded in a flexible film and lifted-off from their native substrate can sustain large deformations thanks to the high flexibility of individual nanowires and to their footprint much smaller than the typical curvature radius.<sup>32–35</sup> Moreover, the lift-off and transfer procedure enables the assembly of free-standing layers of nanowire materials with different bandgaps without any constraint related to lattice-matching or growth conditions compatibility. This novel concept therefore allows for a large design freedom and modularity because it enables a combination of materials with very different physical and chemical properties, which cannot be achieved by monolithic growth. Thanks to the small amount of the active material and the possible reuse of the growth substrate, this technology can also reduce the cost with respect to conventional 2D nitride LEDs. At the same time, a better luminance and stability with respect to current organic flexible technologies can be achieved.

There have been few research works on flexible nanowire LEDs based on inorganic nanowires, including single-crystalline ZnO nanowires grown on indium-tin-oxide- (ITO) coated flexible substrate,<sup>36</sup> GaN/ZnO coaxial nanorod heterostructures,<sup>37</sup> and GaN microrods<sup>38</sup> synthesized on graphene films. Electroluminescence in the visible spectral range was achieved in all these realizations. However, the demonstrated devices present several drawbacks such as the poor flexibility of the ITO layer<sup>36</sup> or the low transmittance of the Ni/Au conductive layer used as a top electrode detrimental for light extraction.<sup>37,38</sup> It should be noted that no demonstration of multilayer flexible nanowire LEDs taking advantage of the above-mentioned design modularity has been done so far.

In this work, we demonstrate large area (several cm<sup>2</sup>) fully flexible blue LEDs based on core/shell InGaN/GaN nanowires grown by MOCVD. Nanowires are embedded into PDMS layers and mechanically lifted from their growth substrate. Conductive transparent electrodes to these composite membranes are realized using silver nanowire networks. The LEDs exhibit rectifying behavior with a low reverse leakage and a light-up voltage around 3 V. The devices show bright blue emission with no performance degradation neither under outward or inward bending down to 3 mm curvature radius nor in time for more than one month storage in ambient conditions without any protecting encapsulation. Fully transparent flexible LEDs with a high optical transmittance (60% at  $\lambda = 530$  nm) are also realized. Finally, we demonstrate for the first time the integration of green and blue LED membranes into a two-layer bicolor nanowire-based flexible LED. The two layers containing InGaN/GaN nanowires with different In contents can be either separately driven to generate green or blue light or simultaneously biased to generate a broad electroluminescence spectrum, which opens the way to develop nanowire-based high brightness flexible white-light displays.

Self-assembled GaN nanowires with lateral {1100} m-plane facets have been grown by catalyst-free MOVPE on c-sapphire substrates. Details on the growth conditions can be found in refs 24 and 39. The base part of the wire is grown at 1040 °C using trimethylgallium and ammonia precursors combined with silane flux to obtain n<sup>+</sup>-doping and to promote the wire

geometry. The silane flux is switched off after about 9 ± 2 μm length to grow a ~ 24 ± 2 μm long nonintentionally doped (n-i-d) GaN part, which however presents an important residual n-doping close to 10<sup>18</sup> cm<sup>-3</sup>. The top part of the wire is surrounded by 7 periods of radial InGaN/GaN quantum wells (QWs) and is covered with a p-doped 120 nm thick GaN shell with a hole concentration in the 10<sup>16</sup>–10<sup>17</sup> cm<sup>-3</sup> range.<sup>40</sup> Figure 1c shows a schematic of the nanowire internal structure.

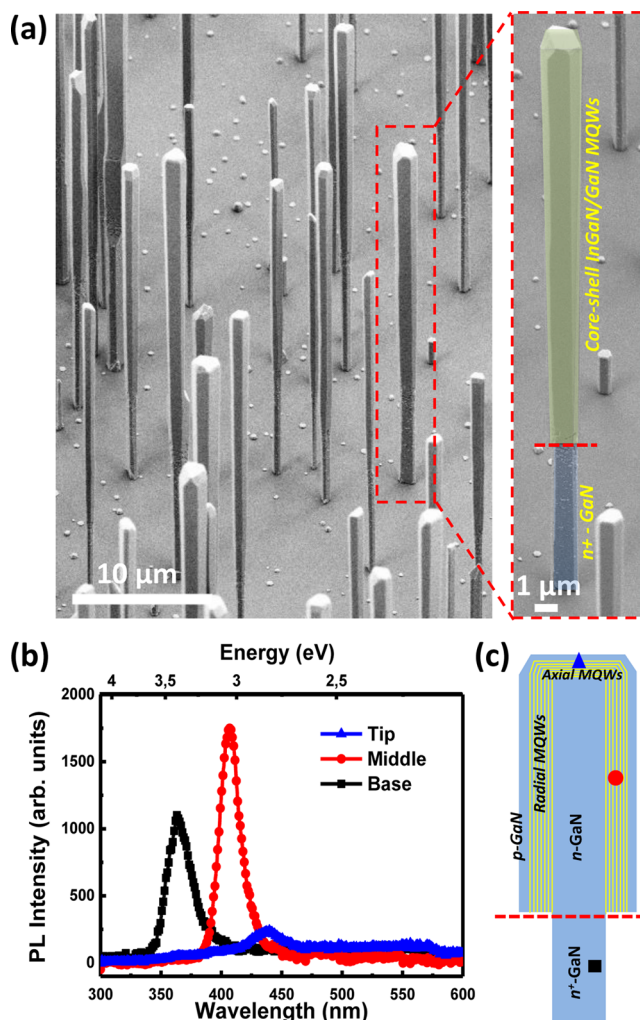


**Figure 1.** (a) SEM image of nanowires from sample A together with a zoomed-in image of an individual wire highlighting in artificial colors the bare n<sup>+</sup>-GaN (base) and the core/shell region. All SEM images are obtained with a tilt angle of 45°. (b) Microphotoluminescence characteristics of a single nanowire for different excitation positions. (c) Schematic of the nanowire structure showing the excitation positions corresponding to the μPL spectra of panel (b).

We note that the used growth conditions allow to control the extension of the core/shell region and to keep the n<sup>+</sup>-doped GaN nanowire pedestal free from radial overgrowth.<sup>39</sup> The diameter of the core/shell region varies from 700 nm to 2 μm. A scanning electron microscopy (SEM) image of the complete nanowire structure of a blue LED sample is shown in Figure 1a together with a close-up image of an individual nanowire showing in artificial colors the core/shell and the base regions.

Three nanowire samples A, B, and C differing only by the QW region have been grown for flexible LED fabrication following the above-described procedure. QWs in sample A

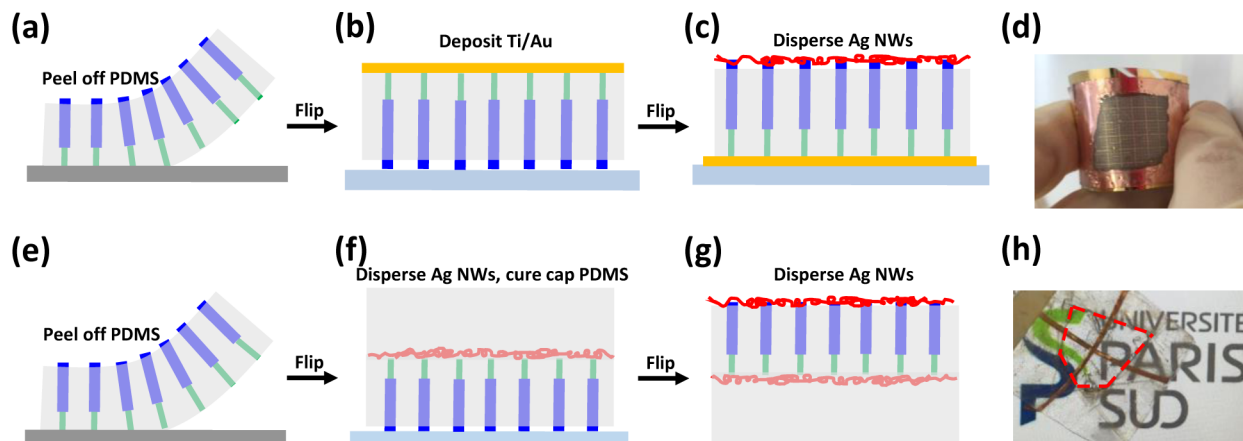


**Figure 2.** Schematic of the fabrication process flow of flexible LEDs based on vertical nitride nanowire arrays. Panels (a–c) illustrate the fabrication steps for semitransparent LEDs with Ti/Au and Ag nanowires as the back and top contacts, respectively. (d) Photo of a semitransparent LED. Panels (e–g) show the process of fully transparent LEDs with Ag nanowires as both back and top contacts. (h) Photo of a transparent LED.

have been grown at  $T = 750\text{ }^{\circ}\text{C}$  under V/III ratio for trimethylgallium and trimethylindium of about 6130 and 2750 respectively, corresponding to a targeted indium content in the QWs about 15% for 120 sccm of trimethylindium flow.<sup>39</sup> The target thicknesses of the InGaN/GaN QW are about 5 nm/10 nm. Sample B has been grown under nominally identical conditions to sample A, however in a different period of time and using a different susceptor, which explains a slight difference in the emission wavelengths between samples A and B. QWs in sample C have been grown at lower temperature of 680  $^{\circ}\text{C}$  and under a stronger trimethylindium flux of 200 sccm in order to increase the In content in the QWs. The target thicknesses of the InGaN/GaN QW are about 2.5 nm/5 nm. On the basis of the emission wavelength, the In content in the C sample is estimated in the 0.25–0.28 range (see Supporting Information). The crystalline structure of the core/shell QWs has been probed by transmission electron microscopy (TEM) and energy dispersive X-ray (EDX) spectroscopy on a reference sample grown under conditions similar to sample A. TEM images reveal a presence of radial (*m*-plane) and axial (semipolar plane and *c*-plane) QW systems. The semipolar QWs located at the nanowire tip have a larger thickness and a higher In content than the *m*-plane QWs coating the nanowire side walls. The QWs on the *c*-plane are distorted and present structural defects. (For more details see the Supporting Information.)

First, the as-grown nanowires were characterized by spatially resolved microphotoluminescence ( $\mu$ PL) spectroscopy. Nanowires were removed from the substrate by ultrasonication in an IPA bath and dispersed onto a thermally oxidized  $\text{SiO}_2/\text{Si}$  substrate. The  $\mu$ PL experiments were carried out at room-temperature using a frequency-doubled cw Ar<sup>2+</sup> ion laser ( $\lambda = 244\text{ nm}$ ). The emission spectra were collected through an objective (20 $\times$ , NA = 0.4) and detected with a HR460 spectrometer and a CCD camera. Figure 1b shows the  $\mu$ PL spectra of an individual wire from sample A for an excitation position located at the base, in the middle, and at the top, respectively. The schematic of the nanowire structure shown in Figure 1c illustrates the three corresponding excitation positions. Three different peaks having different intensities are observed at these regions. The peak at 3.41 eV is detected at the base of the nanowire, corresponding to the near band edge emission of the n-doped GaN segment. In the middle and top

wire parts, two peaks are observed below the GaN bandgap. The low energy peak ( $E = 2.83\text{ eV}$ , fwhm = 0.15 eV) arises from the nanowire extremity, when the laser spot is almost outside the wire hitting only its very top, whereas the high energy peak ( $E = 3.05\text{ eV}$ , fwhm = 0.24 eV) is spread over the whole core/shell region. According to the TEM studies (see Supporting Information), we can attribute the 2.83 and 3.05 eV peaks to the emission of the axial and radial QWs, respectively.<sup>41</sup> Regarding the low energy peak, it can arise from both semipolar and polar QWs at the top of the nanowire (both referred here as “axial”), however the higher defect density of the *c*-plane QWs suggests that the major contribution is given by the semipolar QWs as discussed in the Supporting Information.

The nanowire samples A to C have been used to fabricate flexible LEDs. One major challenge to fabricate high-performance flexible LEDs is the need for a highly conductive, transparent, mechanically flexible contact. ITO, the traditional contact for LEDs, offers both a low sheet resistance and a high optical transmittance, but suffers from brittleness and high cost. Thus, several alternative materials have been investigated to tackle these shortcomings, including conductive polymers,<sup>36,42</sup> carbon nanotubes,<sup>43–45</sup> metal nanoparticles,<sup>46</sup> graphene,<sup>47–51</sup> and metal wires.<sup>52–57</sup> The widespread usage of conductive polymers is hindered by their instability in air ambient and some process incompatibilities.<sup>58</sup> For carbon nanotubes, the coexistence of metallic and semiconducting tubes increases the network sheet resistances.<sup>59</sup> Conformal metal nanoparticle films have been investigated recently as a transparent charge transport layer with additional plasmonic scattering properties.<sup>46</sup> Two-dimensional graphene, one-dimensional metal nanowires and combination of both have been explored as emerging candidates for transparent electrodes satisfying the requirement for a low resistance, a high flexibility, and an optical transparency.<sup>54</sup> In addition, the controllable synthesis and low-cost of these materials further promises their broad use in LEDs and solar cells. In this work, we have chosen the silver nanowire network as a solution for the transparent electrode. To achieve a high quality ohmic contact, silver nanowires are combined with an ultrathin Ni/Au shell deposited directly onto the LED nanowires.

The fabrication steps to produce flexible devices are the following: first, a thin metal shell (Ni/Au 2 nm/2 nm) is

sputtered on the top of the p-GaN region ( $\sim 3 \mu\text{m}$ ) with a photoresist protecting the n-GaN base, followed by a lift-off and a 10 min annealing in air at  $400^\circ\text{C}$ . Then, the GaN nanowire array ( $\sim 33 \mu\text{m}$  in height) is embedded into polydimethylsiloxane (PDMS)<sup>60</sup> with protruding top portions of  $\sim 1 \mu\text{m}$ . The whole layer is peeled off with nanowires maintaining their positions with respect to each other as illustrated in Figure 2a,e. Figure 2 schematizes the fabrication process of two types of devices: semitransparent LEDs (Figure 2a–d) and fully transparent LEDs (Figure 2e–h).

For the semitransparent device fabrication, the PDMS membrane with embedded nanowires is flipped onto an arbitrary holder for the metallization of n-GaN side with Ti/Au (Figure 2b). Next, a flexible substrate (e.g., PET or metal foil) is brought in contact with the metal layer and the whole layer is mounted using silver epoxy. After plasma cleaning of the PDMS residues on the p-GaN side,<sup>61</sup> a metal grid is deposited to facilitate the long-range current spreading and then Ag nanowires<sup>62</sup> are spun coated to form the top transparent electrode (Figure 2c). The device is annealed at  $200^\circ\text{C}$  for 20 min to partly melt silver nanowires together and improve the in-plane conductivity. No encapsulation has been deposited to protect the final device from ambient oxidants and pollutants. Using this process, vertical nanowire array LEDs were successively fabricated on a copper tape (a photo of the final device is shown in Figure 2d).

For the fully transparent devices, Ag nanowires are used for both back and top contacts. As illustrated in Figure 2f, the dispersion of Ag nanowires is followed by the spin-coating and curing of another PDMS capping layer for backside electrical insulation. The whole layer is then flipped back and the process of Ag nanowire coating (Figure 2c) is repeated. Figure 2h shows an example of the transparent LED processed following the (e–g) steps. The boundaries of the active region are marked with a red dashed polygon, while the exterior parts correspond to the plastic scotch tape used for mechanical support. As seen in Figure 2h, the device exhibits a good transparency except for the metallic tape cross deposited before PDMS back capping to access the bottom contact.

Figure 3a shows an SEM image of the surface of a PDMS/nitride nanowire membrane spin-coated with Ag nanowires. A uniform density of Ag nanowires is obtained despite the presence of protruding  $1 \mu\text{m}$  nitride nanowire tips. The zoom-in image in Figure 3b shows that the nitride nanowire tips are well connected with the Ag nanowire network. This coverage provides a good optical transmittance as well as a good ohmic connection to nitride nanowires thanks to the presence of a thin Ni/Au shell on the p-GaN shell. After numerous bending cycles, the Ag nanowires maintain a good contact with the active InGaN/GaN nanowires (SEM observations after 10 bending cycles have not revealed any morphology change). In addition, a thermal annealing at  $200^\circ\text{C}$  for 20 min enables an enhancement of the electrical conductivity<sup>63,64</sup> by melting and fusion of the Ag nanowires, forming a connected Ag network as shown in Figure 3c. This has been confirmed by sheet resistance measurements using a van der Pauw method, conducted on a reference PDMS/PET sample spun-coated with Ag nanowires having the same density as in the flexible LED of Figure 3a. They reveal a decrease from  $39 \Omega/\text{sq}$  in as-deposited sample to  $17 \Omega/\text{sq}$  in annealed sample.

Transparency of the Ag nanowire contacts was characterized on the same reference samples. The transmission is measured

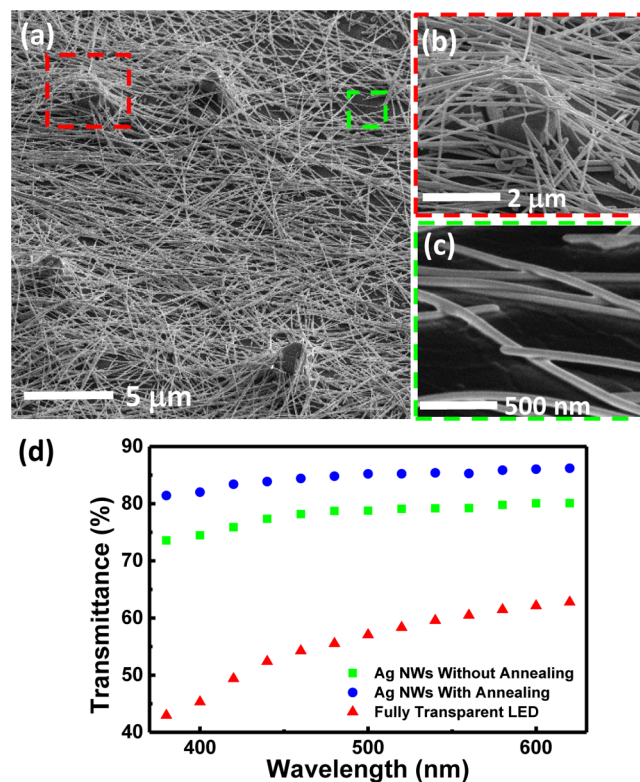


**Figure 3.** (a) SEM image of annealed Ag nanowire network spun-cast on PDMS/nitride nanowire LEDs to form the top contact to Ni/Au coated p-GaN nanowire shells. (b) Higher-magnification SEM image (shown with red dashed rectangle in panel (a)) of a protruding InGaN/GaN nanowire presenting a good coverage by Ag nanowires. (c) SEM image of the region highlighted with a green dashed rectangle in panel (a) showing the Ag nanowire partial melting after annealing. (d) Optical transmittance of a single-layer Ag nanowire film before and after annealing and of a fully transparent LED device.

using a tunable spectral illuminator and a powermeter with a flat spectral response. The transmission spectrum is normalized by the transmission of a bare PDMS/PET substrate. Figure 3d illustrates the optical transmittance of the Ag nanowire films. Values above 80% are achieved after thermal annealing, which increases the transmittance over the whole spectral range (e.g., from 79% for the as-coated to 85% for the annealed film at  $\lambda = 530 \text{ nm}$ ). The transparency of the fully transparent LED has also been characterized as reported in Figure 3d. The LED exhibits a slightly lower transmittance in the short wavelength range than expected from a double Ag nanowire layer due to the absorption in the InGaN/GaN nanowires. However, the transmittance in the green spectral range is higher than 60%.

Electrical characteristics of the flexible nanowire LEDs were investigated by measuring the current–voltage ( $I$ – $V$ ) curves from  $-5$  to  $5 \text{ V}$ , as shown in Figure 4.  $I$ – $V$  characteristic shows a rectifying, diode-like behavior with a turn-on voltage around  $3 \text{ V}$ , above which the current increases rapidly with the bias voltage. The electroluminescence (EL) appears at about  $3 \text{ V}$  bias. To explore the origin of the light emission, voltage-dependent electroluminescence (EL) spectra have been measured at room temperature using a HR460 spectrometer and a CCD camera. The spectra for biases from  $4$  to  $8 \text{ V}$  are shown in the inset of Figure 4. At the lowest voltage, the dominant EL emission is peaked at  $447 \text{ nm}$  in good agreement with the  $\mu\text{PL}$  (Figure 1c) emission of axial QWs. As the voltage

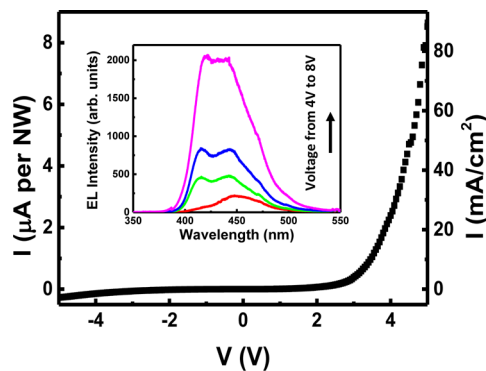


**Figure 4.**  $I$ - $V$  characteristic of the flexible LED normalized to the number of contacted nanowires (left scale) or to the device surface (right scale). Inset presents the room-temperature EL spectra at various applied biases from 4 to 8 V.

increases, a new peak at 415 nm corresponding to the radial QWs appears and its intensity increases. As has been shown in the literature, at low injection the current preferentially goes through the nanowire tips into axial QWs in correspondence to the In-rich region.<sup>30,41,65</sup> Because of the non-negligible resistance of the p-doped GaN shell, at high injection the hole transport in the shell toward axial QWs leads to a potential drop and becomes unfavorable.<sup>30</sup> The injection takes place under the contact thus favoring the emission from the radial QWs.<sup>41</sup> As a result, the EL peak at shorter wavelength becomes more pronounced and a broad emission covering the 400–500 nm range is achieved.

The mechanical properties of the flexible LEDs mounted on a copper tape on PET have been evaluated at a fixed voltage of 5 V as shown in Figure 5. Figure 5a shows a photograph under operation of an unbent device having an active area size of  $15 \times 6.5 \text{ mm}^2$ . The LED exhibits a bright blue emission. Under both outward and inward bending, the device shows no degradation of either current or EL intensity evidencing the electrical reliability of the meshed Ag nanowire networks under deformation. Corresponding photographs with the bending radii of 3.5 mm and 2.5 mm are shown in Figure 5b,c, respectively. Similarly, no appreciable change in either  $I$ - $V$  or EL characteristics has been observed when comparing the performances before and after numerous ( $>10$ ) bending cycles. In addition, the device storage in ambient conditions for more than 30 days has shown no impact on the LED performance. This demonstrates the flexibility, reliability, and stability of the

flexible nanowire LEDs. We stress that in contrast to OLEDs, the nanowire LEDs do not require any encapsulation.

To progress toward flexible display applications, pixels of different colors should be realized. Multicolor device can be achieved by combining flexible LEDs containing different active nanowires. To demonstrate this functionality we have stacked two layers, a semitransparent green LED fabricated from sample C with a transparent blue LED fabricated from sample B as illustrated in Figure 6a. The two flexible LEDs are stacked

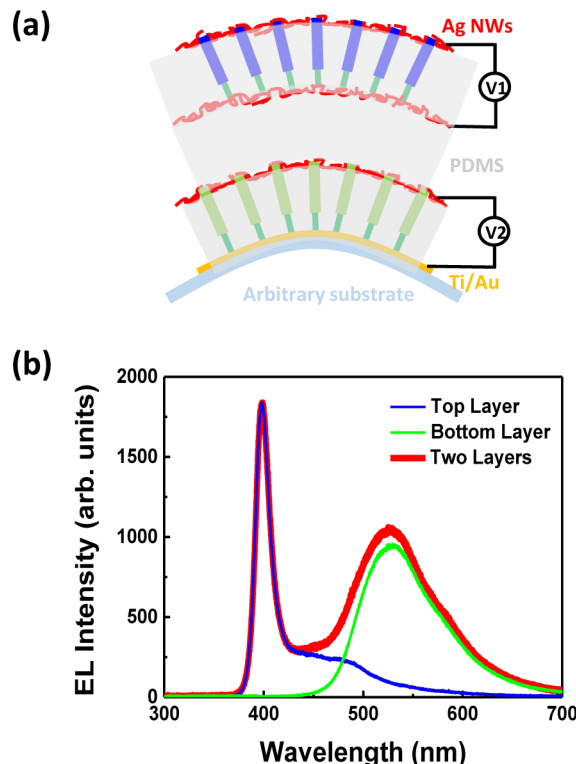


**Figure 6.** (a) Schematic of a two-color nanowire flexible LED. (b) EL spectra of a two-layer flexible LED with a top transparent layer and a bottom semitransparent layer. Three curves show the emission from the top LED (blue curve), from the bottom LED (green curve), and a simultaneous emission from both LEDs (red curve), respectively.

together with an intermediate PDMS layer. Figure 6b shows the EL spectra of the two-layer device for different biasing conditions. Two voltage sources  $V_1$  and  $V_2$  are independently connected to the top and bottom LED layers. In the case  $V_1 = 6$  V and  $V_2 = 0$  V (i.e., only the top layer is biased), the emission

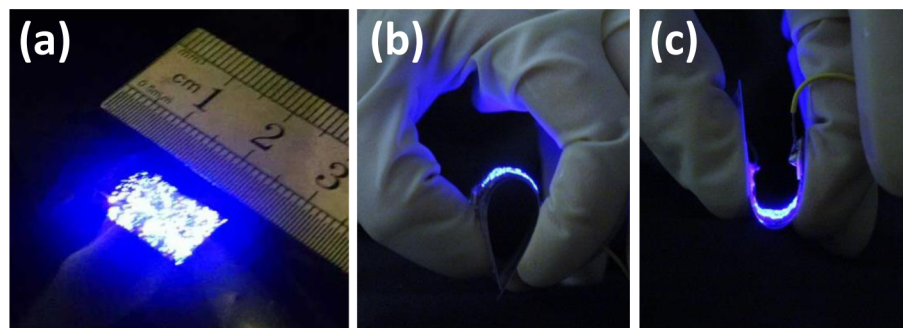


**Figure 5.** Mechanical properties of the flexible LED based on vertical nanowire arrays. Photograph of the LED emitting blue light at curvature radii of (a)  $\infty$ , (b) 3.5 mm, and (c) -2.5 mm.

is detected only in the blue spectral region in correspondence to the EL of the top transparent LED (blue curve in Figure 6b). For  $V_1 = 0$  V and  $V_2 = 7$  V (i.e., only the bottom layer is biased), only green EL is observed from the bottom semitransparent LED (green curve in Figure 6b). Once both of the layers are biased simultaneously with  $V_1 = 6$  V and  $V_2 = 7$  V, the emission covers both blue and green spectral region as presented by the red curve in Figure 6b. The optical transmittance of the top transparent LED is ~60% at the peak emission wavelength of the bottom LED (see red dots in Figure 3d.), so that the blue luminescence of the bottom layer can be efficiently extracted through the top layer. These results demonstrate the feasibility of multilayer flexible LEDs by a mechanical stacking technique. We note that the present approach has potentially no limitations for the number of LED layers except for the residual absorption. Moreover, it allows for an integration of nanowire layers of different semiconductor materials (e.g., nitrides with phosphides or arsenides) as well as for a hybrid integration of blue nitride LEDs with organic devices to achieve RGB emission.

In conclusion, flexible LEDs based on vertical nitride nanowire arrays and transparent Ag nanowire electrodes have been demonstrated. Embedding the inorganic semiconductor nanowires into a polymer matrix ensures the mechanical flexibility, while Ag nanowires provide a reliable electrical contact with high conductivity and optical transmittance. No degradation in current and EL emission was observed in such devices either after bending cycles or after more than 30 days storage in ambient conditions. Using this platform, we demonstrated for the first time the integration of two layers of flexible LEDs with different emission wavelength in the blue and green spectral domains to achieve a color-tunable LED. This technology opens new routes for efficient flexible LED displays and other optoelectronic devices.

## ■ ASSOCIATED CONTENT

### Supporting Information

The Supporting Information is available free of charge on the ACS Publications website at DOI: [10.1021/acs.nanolett.5b02900](https://doi.org/10.1021/acs.nanolett.5b02900).

Structural characterization, characterization of the light emitting diodes B and C used for the two-color device, and Figures S1–S3. ([PDF](#))

## ■ AUTHOR INFORMATION

### Corresponding Authors

\*E-mail: [dai.xing@u-psud.fr](mailto:dai.xing@u-psud.fr).

\*E-mail: [maria.tchernycheva@u-psud.fr](mailto:maria.tchernycheva@u-psud.fr).

### Notes

The authors declare no competing financial interest.

## ■ ACKNOWLEDGMENTS

This work has been partially financially supported by ANR “Investissement d’Avenir” programs “GaNeX” (ANR-11-LABX-2014) and “NanoSaclay” (ANR-10-LABX-0035), by ANR-14-CE26-0020-01 project “PLATOFIL” and by EU ERC project “NanoHarvest” (Grant 639052). The device processing has been performed at CTU-IEF-Minerve technological platform, member of the Renatech RTB network.

## ■ REFERENCES

- (1) Sasabe, H.; Kido, J. *J. Mater. Chem. C* **2013**, *1* (9), 1699–1707.
- (2) Brütting, W.; Frischeisen, J.; Schmidt, T. D.; Scholz, B. J.; Mayr, C. *Phys. Status Solidi A* **2013**, *210* (1), 44–65.
- (3) Thejokalyani, N.; Dhoble, S. J. *Renewable Sustainable Energy Rev.* **2014**, *32*, 448–467.
- (4) Zhang, Y.; Lee, J.; Forrest, S. R. *Nat. Commun.* **2014**, *5*, 5008.
- (5) Aziz, H.; Popovic, Z. D.; Hu, N.-X.; Hor, A.-M.; Xu, G. *Science* **1999**, *283* (5409), 1900–1902.
- (6) So, F.; Kondakov, D. *Adv. Mater.* **2010**, *22* (34), 3762–77.
- (7) Chang, M.-H.; Das, D.; Varde, P. V.; Pecht, M. *Microelectron. Reliab.* **2012**, *52* (5), 762–782.
- (8) *Organic Light-Emitting Materials and Devices*, 2nd ed.; Taylor & Francis Group: New York, 2015; Vol. 3.
- (9) Lee, C. W.; Lee, J. Y. *Adv. Mater.* **2013**, *25* (38), 5450–4.
- (10) Herrnsdorf, J.; McKendry, J. J. D.; Zhang, S.; Xie, E.; Ferreira, R.; Massoubre, D.; Zuhdi, A. M.; Henderson, R. K.; Underwood, I.; Watson, S.; Kelly, A. E.; Gu, E.; Dawson, M. D. *IEEE Trans. Electron Devices* **2015**, *62* (6), 1918–1925.
- (11) Jiang, H. X.; Lin, J. Y. *Opt. Express* **2013**, *21* (S3), A475–84.
- (12) Narukawa, Y.; Ichikawa, M.; Sanga, D.; Sano, M.; Mukai, T. *J. Phys. D: Appl. Phys.* **2010**, *43* (35), 354002.
- (13) Lee, S. Y.; Park, K.-I.; Huh, C.; Koo, M.; Yoo, H. G.; Kim, S.; Ah, C. S.; Sung, G. Y.; Lee, K. J. *Nano Energy* **2012**, *1* (1), 145–151.
- (14) Goßler, C.; Bierbrauer, C.; Moser, R.; Kunzer, M.; Holc, K.; Pletschen, W.; Köhler, K.; Wagner, J.; Schwaerzel, M.; Ruther, P.; Paul, O.; Neef, J.; Keppeler, D.; Hoch, G.; Moser, T.; Schwarz, U. T. *J. Phys. D: Appl. Phys.* **2014**, *47* (20), 205401.
- (15) Seo, J.-H.; Li, J.; Lee, J.; Gong, S.; Lin, J.; Jiang, H.; Ma, Z. *IEEE Photonics J.* **2015**, *7* (2), 1–7.
- (16) Chun, J.; Hwang, Y.; Choi, Y.-S.; Jeong, T.; Baek, J. H.; Ko, H. C.; Park, S.-J. *IEEE Photonics Technol. Lett.* **2012**, *24* (23), 2115–2118.
- (17) Choi, J. H.; Cho, E. H.; Lee, Y. S.; Shim, M.-B.; Ahn, H. Y.; Baik, C.-W.; Lee, E. H.; Kim, K.; Kim, T.-H.; Kim, S.; Cho, K.-S.; Yoon, J.; Kim, M.; Hwang, S. *Adv. Opt. Mater.* **2014**, *2* (3), 267–274.
- (18) Espinosa, H. D.; Bernal, R. A.; Minary-Jolandan, M. *Adv. Mater.* **2012**, *24* (34), 4656–75.
- (19) Glas, F. *Phys. Rev. B: Condens. Matter Mater. Phys.* **2006**, *74* (12), 121302.
- (20) Chesi, J.; Gradelak, S. *J. Nanophotonics* **2014**, *8* (1), 083095.
- (21) Li, S.; Waag, A. *J. Appl. Phys.* **2012**, *111* (7), 071101.
- (22) Kang, M. S.; Lee, C.-H.; Park, J. B.; Yoo, H.; Yi, G.-C. *Nano Energy* **2012**, *1* (3), 391–400.
- (23) Qian, F.; Li, Y.; Gradečák, S.; Wang, D.; Barrelet, C. J.; Lieber, C. M. *Nano Lett.* **2004**, *4* (10), 1975–1979.
- (24) Koester, R.; Hwang, J.-S.; Salomon, D.; Chen, X.; Bougerol, C.; Barnes, J.-P.; Dang, D. L. S.; Rigutti, L.; de Luna Bugallo, A.; Jacopin, G.; Tchernycheva, M.; Durand, C.; Eymery, J. *Nano Lett.* **2011**, *11* (11), 4839–4845.
- (25) Tchernycheva, M.; Messanvi, A.; de Luna Bugallo, A.; Jacopin, G.; Lavenus, P.; Rigutti, L.; Zhang, H.; Halioua, Y.; Julien, F. H.; Eymery, J.; Durand, C. *Nano Lett.* **2014**, *14* (6), 3515–20.
- (26) McAlpine, M. C.; Friedman, R. S.; Jin, S.; Lin, K.-h.; Wang, W. U.; Lieber, C. M. *Nano Lett.* **2003**, *3* (11), 1531–1535.
- (27) Guo, W.; Zhang, M.; Banerjee, A.; Bhattacharya, P. *Nano Lett.* **2010**, *10* (9), 3355–9.
- (28) Kuykendall, T. R.; Schwartzberg, A. M.; Aloni, S. *Adv. Mater.* **2015**, DOI: [10.1002/adma.201500522](https://doi.org/10.1002/adma.201500522).
- (29) Nguyen, H. P.; Zhang, S.; Connie, A. T.; Kibria, M. G.; Wang, Q.; Shih, I.; Mi, Z. *Nano Lett.* **2013**, *13* (11), 5437–42.
- (30) Tchernycheva, M.; Lavenus, P.; Zhang, H.; Babichev, A. V.; Jacopin, G.; Shahmohammadi, M.; Julien, F. H.; Ciechonski, R.; Vesco, G.; Kryliouk, O. *Nano Lett.* **2014**, *14* (5), 2456–65.
- (31) Limbach, F.; Hauswald, C.; Lahmann, J.; Wolz, M.; Brandt, O.; Trampert, A.; Hanke, M.; Jahn, U.; Calarco, R.; Geelhaar, L.; Riechert, H. *Nanotechnology* **2012**, *23* (46), 465301.
- (32) Reimer, M. E.; Bulgarini, G.; Akopian, N.; Hocevar, M.; Bavinck, M. B.; Verheijen, M. A.; Bakkers, E. P. A. M.; Kouwenhoven, L. P.; Zwillaer, V. *Nat. Commun.* **2012**, *3*, 737.

- (33) Plass, K. E.; Filler, M. A.; Spurgeon, J. M.; Kayes, B. M.; Maldonado, S.; Brunschwig, B. S.; Atwater, H. A.; Lewis, N. S. *Adv. Mater.* **2009**, *21* (3), 325–328.
- (34) Spurgeon, J. M.; Boettcher, S. W.; Kelzenberg, M. D.; Brunschwig, B. S.; Atwater, H. A.; Lewis, N. S. *Adv. Mater.* **2010**, *22* (30), 3277–81.
- (35) Fan, Z.; Razavi, H.; Do, J.-w.; Moriaki, A.; Ergen, O.; Chueh, Y.-L.; Leu, P. W.; Ho, J. C.; Takahashi, T.; Reichert, L. A.; Neale, S.; Yu, K.; Wu, M.; Ager, J. W.; Javey, A. *Nat. Mater.* **2009**, *8* (8), 648–653.
- (36) Nadarajah, A.; Word, R. C.; Meiss, J.; Konenkamp, R. *Nano Lett.* **2008**, *8*, 534–537.
- (37) Lee, C.-H.; Kim, Y.-J.; Hong, Y. J.; Jeon, S.-R.; Bae, S.; Hong, B. H.; Yi, G.-C. *Adv. Mater.* **2011**, *23* (40), 4614–4619.
- (38) Chung, K.; Beak, H.; Tchoe, Y.; Oh, H.; Yoo, H.; Kim, M.; Yi, G.-C. *APL Mater.* **2014**, *2* (9), 092512.
- (39) Koester, R.; Hwang, J. S.; Durand, C.; Dang Dle, S.; Eymery, J. *Nanotechnology* **2010**, *21* (1), 015602.
- (40) Tchoultian, P.; Donatini, F.; Levy, F.; Dussaigne, A.; Ferret, P.; Pernot, J. *Nano Lett.* **2014**, *14* (6), 3491–8.
- (41) Jacopin, G.; De Luna Bugallo, A.; Lavenus, P.; Rigutti, L.; Julien, F. H.; Zagone, L. F.; Kociak, M.; Durand, C.; Salomon, D.; Chen, X. J.; Eymery, J.; Tchernycheva, M. *Appl. Phys. Express* **2012**, *5* (1), 014101.
- (42) Na, S.-I.; Kim, S.-S.; Jo, J.; Kim, D.-Y. *Adv. Mater.* **2008**, *20* (21), 4061–4067.
- (43) Wu, Z.; Chen, Z.; Du, X.; Logan, J. M.; Sippel, J.; Nikolou, M.; Kamaras, K.; Reynolds, J. R.; Tanner, D. B.; Hebard, A. F.; Rinzel, A. G. *Science* **2004**, *305* (5688), 1273–1276.
- (44) Pasquier, A. D.; Unalan, H. E.; Kanwal, A.; Miller, S.; Chhowalla, M. *Appl. Phys. Lett.* **2005**, *87* (20), 203511.
- (45) Yu, G.; Cao, A.; Lieber, C. M. *Nat. Nanotechnol.* **2007**, *2* (6), 372–7.
- (46) Sugnaux, C.; Mallorquí, A. D.; Herriman, J.; Klok, H.-A.; Morral, A. F. i. *Adv. Funct. Mater.* **2015**, *25* (25), 3958–3965.
- (47) Park, J. U.; Nam, S.; Lee, M. S.; Lieber, C. M. *Nat. Mater.* **2011**, *11* (2), 120–5.
- (48) Chen, J. H.; Jang, C.; Xiao, S.; Ishigami, M.; Fuhrer, M. S. *Nat. Nanotechnol.* **2008**, *3* (4), 206–9.
- (49) Cai, W.; Zhu, Y.; Li, X.; Piner, R. D.; Ruoff, R. S. *Appl. Phys. Lett.* **2009**, *95* (12), 123115.
- (50) Li, Z.; Kang, J.; Zhang, Y.; Liu, Z.; Wang, L.; Lee, X.; Li, X.; Yi, X.; Zhu, H.; Wang, G. *J. Appl. Phys.* **2013**, *113* (23), 234302.
- (51) Zhang, H.; Babichev, A. V.; Jacopin, G.; Lavenus, P.; Julien, F. H.; Yu, Egorov, A.; Zhang, J.; Pauperté, T.; Tchernycheva, M. *J. Appl. Phys.* **2013**, *114* (23), 234505.
- (52) Lee, J.-Y.; Connor, S. T.; Cui, Y.; Peumans, P. *Nano Lett.* **2008**, *8* (2), 689–692.
- (53) De, S.; Higgins, T. M.; Lyons, P. E.; Doherty, E. M.; Nirmalraj, P. N.; Blau, W. J.; Boland, J. J.; Coleman, J. N. *ACS Nano* **2009**, *3* (7), 1767–1774.
- (54) Lee, M. S.; Lee, K.; Kim, S. Y.; Lee, H.; Park, J.; Choi, K. H.; Kim, H. K.; Kim, D. G.; Lee, D. Y.; Nam, S.; Park, J. U. *Nano Lett.* **2013**, *13* (6), 2814–21.
- (55) Xu, F.; Zhu, Y. *Adv. Mater.* **2012**, *24* (37), 5117–22.
- (56) Jeong, G.-J.; Lee, J.-H.; Han, S.-H.; Jin, W.-Y.; Kang, J.-W.; Lee, S.-N. *Appl. Phys. Lett.* **2015**, *106* (3), 031118.
- (57) Hu, L.; Kim, H. S.; Lee, J.-Y.; Peumans, P.; Cui, Y. *ACS Nano* **2010**, *4* (5), 2955–2963.
- (58) Billingham, N. C.; Calvert, P. D.; Foot, P. J. S.; Mohammad, F. *Polym. Degrad. Stab.* **1987**, *19* (4), 323–341.
- (59) Che, Y.; Wang, C.; Liu, J.; Liu, B.; Lin, X.; Parker, J.; Beasley, C.; Wong, H. S. P.; Zhou, C. *ACS Nano* **2012**, *6* (8), 7454–7462.
- (60) PDMS SYLGARD 184 silicone was purchased from Dow Corning. A weight ratio of PDMS curing agent and base (1:10) was mixed and spun-coated on the as-grown substrate, followed by curing at 80 °C for one hour.
- (61) PDMS is etched in a mixture of CF<sub>4</sub>/O<sub>2</sub> (3:1) at 50 mTorr with RF power of 270 W for 1 min.
- (62) Ag nanowires were purchased from Seashell Technology (AgNW-115) with average lengths of 5–15 μm and average diameter of 50–70 nm. Ag nanowires are shipped in IPA solution with the concentration of 0.1 mg/mL.
- (63) Madaria, A. R.; Kumar, A.; Ishikawa, F. N.; Zhou, C. *Nano Res.* **2010**, *3* (8), 564–573.
- (64) Langley, D.; Giusti, G.; Mayousse, C.; Celle, C.; Bellet, D.; Simonato, J. P. *Nanotechnology* **2013**, *24* (45), 452001.
- (65) Hong, Y. J.; Lee, C. H.; Yoon, A.; Kim, M.; Seong, H. K.; Chung, H. J.; Sone, C.; Park, Y. J.; Yi, G. C. *Adv. Mater.* **2011**, *23* (29), 3284–8.